

Replacing conventional brittleness indices determination with new attributes employing true hydrofracturing mechanism

Ritesh Kumar Sharma^{†*}, Satinder Chopra[†] and Larry R. Lines⁺

[†]TGS, Calgary; ⁺University of Calgary, Canada

Summary

Shale resource plays are associated with low permeability, and hence hydraulic fracturing is required for their stimulation and production. Even though considerable nonuniqueness exists in identifying favorable zones for hydraulic fracturing, geophysicists seem to be avid followers of Rickman et al.'s (2008), brittleness criteria of low Poisson's ratio and high Young's modulus, proposed a decade ago. In this study, we highlight the challenges in following such a criterion, and propose a new attribute that makes use of strain energy density and fracture toughness. While the former controls fracture initiation, the propagation of fractures is governed by the latter. As hydraulic fracturing comprises both these properties, we firmly believe that the new proposed attribute could be used to highlight the favorable intervals for fracturing. Core data, well-log curves along with mud-logs have been used to authenticate the proposed attribute. Finally, we implement it on the seismic data and observe encouraging results.

Introduction

Hydraulic fracturing is essential for enhancing the production from shale resource plays with low permeability. Since brittle rocks fracture much better than ductile rocks, identification of pockets in organic shale formations that exhibit higher brittleness has become the focus of our industry nowadays. To quantify brittleness, different methods have evolved over time, that are based on (a) the mechanical properties of rocks, (b) their composition, and (c) the use of elastic parameters characterizing those rocks. The methods in the first two categories make measurements or carry-out analysis on rock samples and use that information to compute brittleness measures. Methods under category (c) can determine elastic parameters from seismic data and after appropriate corrections compute a brittleness measure. As these methods can yield spatial distribution of brittleness from 3D seismic data, they are found to be attractive and are usually followed.

By making ultrasonic measurements in the laboratory on rock samples from the Barnett Shale and deriving the Young's modulus and Poisson's ratio, Rickman et al. (2008) used the average of the normalized Young's modulus and Poisson's ratio and proposed the following empirical equation for evaluating the brittleness index (BI) of a rock formation.

$$BI = 0.5 \left\{ \left[\frac{E - E_{min}}{E_{max} - E_{min}} \right] + \left[\frac{\nu - \nu_{max}}{\nu_{min} - \nu_{max}} \right] \right\} \quad (1)$$

where E is the Young's modulus and ν is the Poisson's ratio. E_{min} , E_{max} and ν_{min} , ν_{max} are the minimum and maximum values of Young's modulus and Poisson's ratio, respectively. In the above definition, the criterion of low ν and high E is followed for identifying the brittle zones. While the former reflects the ability of a rock to fail under stress, the latter helps a fracture remain open. This criterion has been used quite often for stimulating shale reservoirs where a negative correlation between E and ν exists. In a scenario, when positive correlation between these two

properties holds true, it is challenging to select the intervals corresponding to low ν and high E . We cite here an example from the Montney area in British Columbia, Canada, with a crossplot of E and ν computed from well data as shown in Figure 1. Notice the positive correlation between these two parameters. When these two attributes are combined as per equation (1), the computed BI does not show much variation as seen in Figure 1b (right track). Based on this BI , it is not possible to differentiate between Upper and Lower Montney, considering their fracturing characteristics. However, it is well known that Upper Montney is more favorable for fracturing (Sharma and Chopra, 2016). Thus, a positive relationship of E with ν that exists for different shale resource plays (Miskimins et. Al., 2012; Zhang and Bentley, 2005; Chopra and Sharma, 2017), makes it difficult for geoscientists to locate favorable drilling zones. Additionally, Rickman et al.'s (2008) proposal received opposition from engineers and geomechanists, as they were critical of the very basis of the definition of brittleness used, which they thought was being confused with better fracability. The correlation of high E with brittleness gets its main opposition from the geomechanics and engineering domains due to a few concerns that we discuss next.

Brittleness determination in geomechanics

As per geomechanics, when a rock sample of a brittle material is loaded, it can fail in a catastrophic way and has a relatively short plastic deformation in comparison with ductile material. Associating high E with brittleness may not always be true as can be understood by considering three different scenarios depicted in Figure 2. Further, it is commonly known that rocks deform in a brittle manner at low confining stresses and become ductile beyond a certain level. This conclusion has been confirmed by the experimental works done by different researchers. Lutz et al. (2010) and Yagiz (2009) studied the impact of confinement of rock brittleness and obtained results as shown in Figure 3a and b. They found that the failure behavior of a material is indeed strongly dependent on the magnitude of confinement. As per the interpretation of their experimental works, it is obvious that more brittle rock failure occurs at lower confinement pressures and vice-versa. It is interesting to observe that while the higher confinement leads to a ductile failure, it is associated with high E . Knowing that BI combines both E and ν , now it is vital to analyze the effect of confinement pressure on the latter. By using experimental data from Haynesville Shale in Louisiana, US and Longmaxi Shale in southern Sichuan Basin, China, Hu et al. (2015) studied the variation of E and ν with confining pressure. They concluded that E increases linearly with confining pressure (as expected) for both shales (Figure 4a and b). However, no obvious relationship between Poisson's ratio and confining pressure was found as shown therein. Thus, the increasing confinement pressure leads to the higher values of BI . Similar

observations were made by Holt et al. (2011), where the authors first define brittleness in terms of elastic and plastic deformation as shown in Figure 5a. They also compute BI proposed by Rickman et al., and crossplot both the brittleness indices with the confining pressure as shown in Figure 5b and c to quantify their relationships. Notice, while the $BI_{Rickman}$ is seen to be increasing with increasing confining stress, the BI proposed by Holt et al. (2011), exhibits a negative correlation with confining stress which is expected. Such a discussion points to an important flaw in brittleness computation via Rickman et al.'s (2008) approach in that it ignores the confining stress that the rocks are under at all times, and hence ignores the true mechanism of hydraulic fracturing. Therefore, it is advisable to revisit the hydraulic fracturing process.

Strain energy density (SED)

Let us turn to the basics of hydraulic fracturing of rocks which entails the initiation of fractures and their propagation. To initiate a fracture, priority should be given to a material which absorbs less energy before it gets fractured. Once the fracture is initiated, the stress state within the rock gets disturbed due to stress concentration at the crack tip. A rock can withstand fracture tip stresses up to a critical value, which is referred to as the critical stress intensity factor; this ability of a rock to resist fracturing and propagation of preexisting fractures is known as *fracture toughness*. Rocks with low fracture toughness promote fracture propagation. Thus, the amount of energy that a formation consumes in the fracture initiation process as well as its propagation must be considered in identifying the favorable zones to be fractured. This said, now the main challenge is how to estimate them in the geophysical domain.

When a subsurface rock is being acted upon by fluid injection during hydraulic fracturing, the fluid does work on the rock. This work is stored in the rock in the form of elastic strain energy and comprises components that cause volume changes as well as distortion by way of angular change. While the normal strains cause a change in volume, the distortion is caused by shear strain. The elastic strain energy per unit volume of the rock is referred to as strain energy density (SED) and for a cube of rock is given as

$$U_{tot} = \frac{1}{2E} (\sigma_x^2 + \sigma_y^2 + \sigma_z^2) - \frac{\nu}{E} (\sigma_x\sigma_y + \sigma_x\sigma_z + \sigma_y\sigma_z) + \frac{1}{2\mu} (\tau_{xy}^2 + \tau_{xz}^2 + \tau_{yz}^2). \quad (2)$$

Due to the tensile fracture (no shear stress) mode being prevalent in hydraulic fracturing, the last term on the right-hand side can be ignored, and the resulting equation shows the importance of principal stresses in identifying the favorable zone for fracturing. As their subsurface measurement is an arduous task, equation (2) can be simplified for hydrostatic condition and used for computation of SED , which is a measure of the energy absorbed by the formation and is related to the area under the stress-strain curve.

Fracture toughness (FT)

FT can be determined in different ways, both direct and indirect. The direct way is to make measurements on rock samples, which is more difficult and more complex than other tests of rock mechanical properties. Therefore, a correlation of FT with

Young's modulus, Poisson's ratio, tensile strength and compressive strength have been derived from experimental data of different types of rocks (Barry et al., 1992). Sierra et al. (2010) published experimental data showing the relationship between FT and tensile strength, compressive strength, Young's modulus and Poisson's ratio for Woodford shale.

That rocks resist the propagation of preexisting cracks being common knowledge, a minimum pressure is required to overcome this resistance and make a fracture grow. Thus, the minimum pressure required to grow the fracture can be correlated with FT , as the higher the FT , the higher the required minimum pressure will be. If somehow this pressure is estimated, it can be used as a proxy for FT . There are two different ways FT could be estimated in the geophysical domain. One way is to use its relationship with P-wave velocity and Young's modulus, and then take their RMS average. The second way is to estimate the minimum pressure required for fracture propagation. Based on the theory proposed by Griffith (1920, 1924) to explain the rupture of brittle, elastic materials, Sack (1946) predicted the minimum pressure (critical) necessary to extend a fracture in a rock for hydraulic fracturing, considering penny shaped cracks as

$$P_c = \sqrt{\frac{\pi\alpha E}{2(1-\nu^2)C}} \quad (3)$$

where α is the specific surface energy of the rock, and C is the crack length. A relevant assumption about the crack length simplifies equation (3) and allow us to compute the minimum pressure using well-log data or seismic data.

Synthesis of a new attribute

Now that we have described both FT and the SED , which is a measure of the energy absorbed by the formation before fracturing, we frame up a new attribute for which we have coined the term *hydraulic fracturing coefficient* (HFC). We compute it as the average of the normalized strain energy density (SED_{norm}) and normalized fracture toughness (FT_{norm}) and written as

$$HFC = \frac{1}{2}(SED_{norm} + FT_{norm}), \text{ where } SED_{norm} = \frac{SED_{max} - SED}{SED_{max} - SED_{min}} \text{ and } FT_{norm} = \frac{FT_{max} - FT}{FT_{max} - FT_{min}} \quad (4)$$

Authentication: To validate the proposed attribute we make use of the experimental data published by Hu et al. (2015) where test results (Table 3.2) were given in terms of Young's modulus, Poisson's ratio, confining pressure, compressive strength, peak strain and residual strain for data samples from Haynesville Shale, Eagle Ford Shale, Barnett Shale and Longmaxi Shale. Given these parameters, it is easy to compute $BI_{Rickman}$ and HFC . To authenticate their applicability for highlighting favorable zones for fracturing, we crossplot them with the compressive strength (CS) as shown in Figure 6a and b. As a material with higher strength is not easy to fracture, an inverse linear relationship between strength and an indicator of fracability is anticipated. Notice that $BI_{Rickman}$ shows an increasing trend with increasing CS which is not expected and hence cannot be treated as an indicator of fracability. HFC on the other hand exhibits a decreasing trend with increasing CS . Thus, it can be concluded that the proposed

attribute better accounts for the impact of strength on the fracability analysis. Again, using the experimental data from Hu et al. (2015) (Table 3.1) as well as the available XRD data, we went ahead and computed BI_{mineral} and BI_{Rickman} . To check how relevant these attributes are, we crossplotted them with compressive strength as shown in Figure 7. Notice, both BI_{mineral} and BI_{Rickman} show an increasing trend with CS , whereas HFC shows a decreasing trend. The inverse linear-trend between HFC and compressive strength of the rock samples from different shale plays lends confidence that it is indeed more relevant and appropriate for hydraulic fracture analysis.

Application to real data: To implement the proposed attribute we picked up the dipole sonic and density log curves for a well from the Delaware Basin, where the zone of interest is from the Bone Spring Formation to the Mississippian Formation. First, we compute E and ν using well-log curves and crossplot them as shown in Figure 8. While the shallow interval from Bone Spring to Wolfcamp exhibits a positive trend (blue), a mixed trend is noticed over an interval from Wolfcamp to Mississippian (red and cyan). It is challenging to identify the favorable zones that could be fractured by following Rickman et al.'s (2008) criteria.

To overcome this problem, we compute SED and FT using well-log data and crossplot them as shown in Figure 9. The cluster points exhibit a nonlinear trend, which is analogous to the one typically seen on P-impedance versus V_p/V_s crossplots. Clusters of data points with different combinations of SED and FT have been enclosed in colored ellipses (Figure 9a), and back-projected on well log curves shown in Figure 9b. We notice that the shallow interval from Bone Spring to Wolfcamp exhibits high FT and low SED , and the deeper interval for Barnett Shale is associated with an opposite combination. Low SED and high FT values imply that the interval is amenable to fracture initiation but not to propagation.

We bring in the available mud log information to understand these results. Low SED or less energy for initiation is supported by lower compressive strength expected in shallower intervals. Higher FT or more resistance to fracture propagation in this shallow interval is due to the higher percentage of limestone in this interval (as seen on the mud log strip shown in 9b).

Similarly, low FT and high SED observed for the deeper interval would absorb more energy before getting fractured, as its strength has increased with depth.

The mud log strip indicates the presence of clay-rich shale in this interval and hence lower resistance to fracture propagation. Both these intervals are not recommended for fracturing in the context of our broad zone of interest, as lower values of HFC are seen on the curve plotted alongside the other two in Figure 9b. Higher values of HFC , which come from an optimal combination of FT and SED are observed for an interval within the Wolfcamp (greenish ellipse on crossplot), which is essentially a limy shale (mud log strip). What we conclude from this is that a small proportion of limestone within the shale offers a suitable condition for fracture initiation and propagation. Needless to mention, this interval has been heavily stimulated for production. With this convincing observation we went ahead and implemented its application on seismic data.

Figure 10 shows the HFC section along an arbitrary line passing through different wells. Hot colors represent higher values of HFC . The interpretation of this section matches very well to the facies section generated using a Bayesian approach based on the neutron-porosity and density-porosity attributes derived seismically.

Conclusions

The different methods of brittleness determination being used in the industry, while applicable to certain subsurface rock formations, are not suitable for others. We pointed out the shortcomings of some of these methods, and then went on to describe a new attribute we call HFC , that makes use of fracture toughness and strain energy density and could be used alternatively. We authenticate the proposed attribute with the help of core data, demonstrate its application to the available data in the Delaware Basin, and exhibit how it provides convincing interpretation on well data and mud-log data. Finally, we implement it on seismic data and observe encouraging results. More applications of this attribute will be discussed in the formal presentation.

Acknowledgements

We wish to thank TGS for encouraging this work and for the permission to present and publish it. The well data used in this work was obtained from the TGS Well Data Library and is gratefully acknowledged.

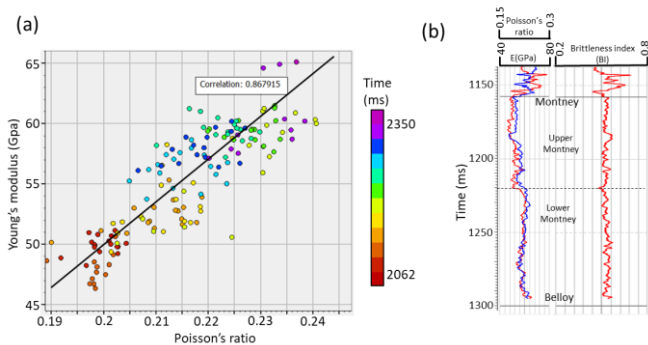


Figure 1: (a) Crossplot between Poisson's ratio and Young's modulus for well log data shown in (b) from the Montney area in British Columbia, Canada. A positive correlation is seen between the two parameters, contrary to the Rickman et al.(2008) criteria. (b) Well log curves for the Montney area well brittleness index curve seen in (b).

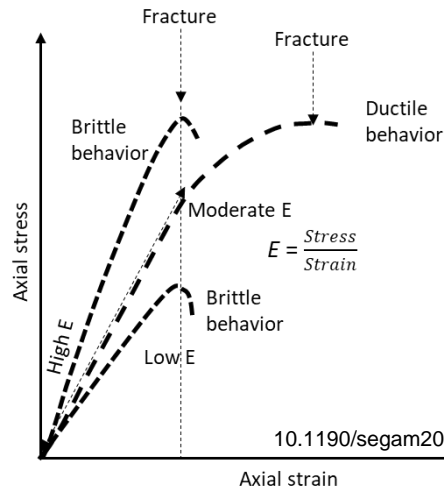


Figure 2: Brittle versus ductile behavior of rock samples as seen on a stress-strain graph, which is independent of Young's modulus.

Replacing conventional brittleness indices determination with new attributes

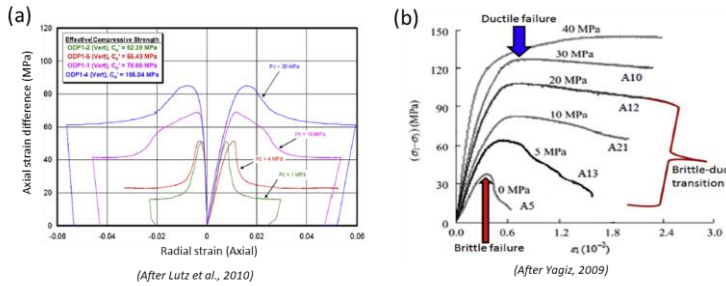


Figure 3: Axial stress difference plotted as a function of strain measurements from (a) four, and (b) six different triaxial tests.

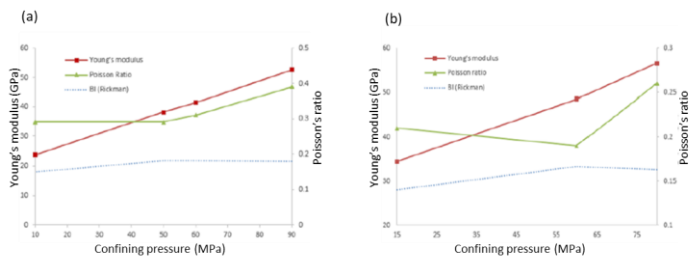


Figure 4: Crossplot between confining pressure and Young's modulus (red) as well as Poisson's ratio (green) for (a) Haynesville shale samples, and (b) Longmaxi shale samples. (After Hu et al., 2015).

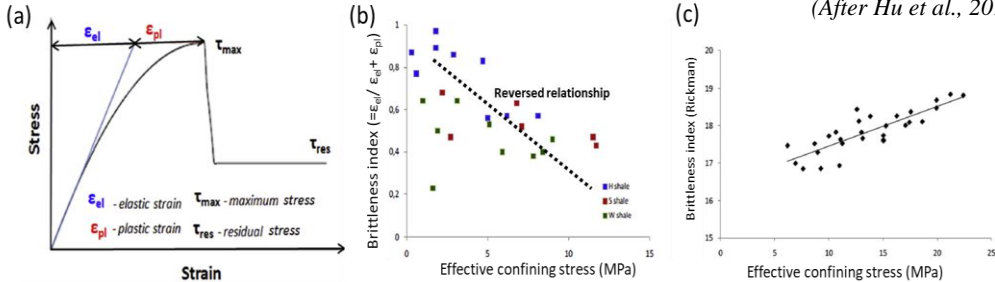


Figure 5: (a) A generic crossplot between measured stress and strain depicting how the brittleness index may be estimated. Crossplot between (b) effective confining stress at failure from triaxial tests on three different shale samples from the North Sea and brittleness index computed using equation 2. (c) effective confining stress based on ultrasonic measurements during hydrostatic loading of a shale sample from the North Sea and brittleness index computed using equation 1. (After Holt et al., 2011)

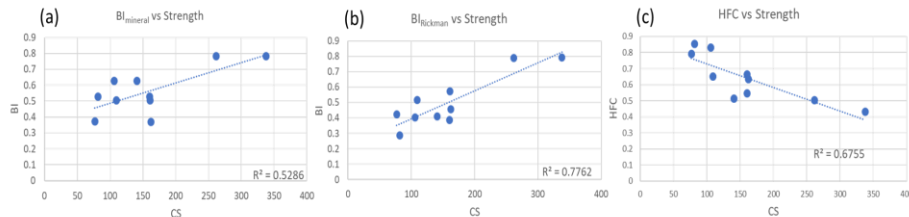


Figure 7: Crossplots between compressive strength and (a) $BI_{mineral}$, (b) $BI_{Rickman}$, and (c) hydraulic fracturing coefficient (HFC). Notice that both brittleness indices in (a) and (b) show an increasing trend, but HFC shows a decreasing trend in (c), which is as per our expectation.

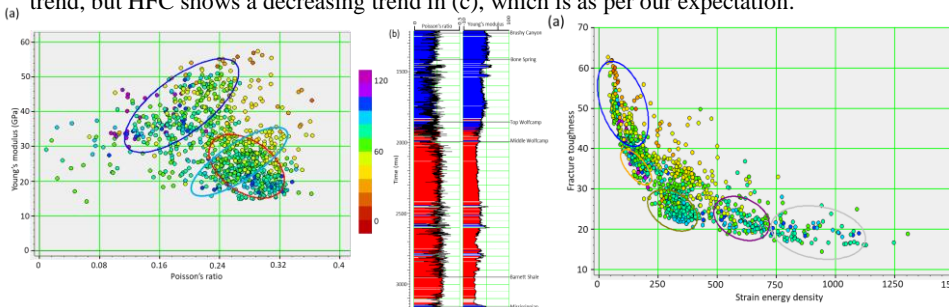


Figure 8: (a) Crossplot between Young's modulus and Poisson's ratio for well log data from Delaware Basin. Different trends seen on this crossplot make it challenging to identify the fracturing zones in our zones of interest. While a positive correlation is seen for the shallow interval, a mixed type of correlation is noticed for the deeper zone as shown in (b), where the back projection of cluster points within different colored polygons on to the well curves is shown.

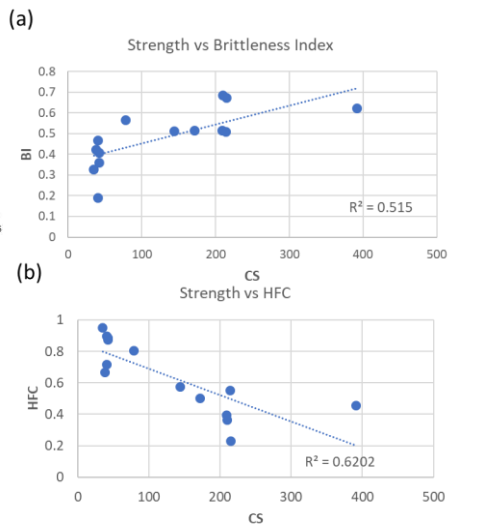


Figure 6: Crossplots between (a) BI (Rickman) and compressive strength, (b) HFC and compressive strength. (Data from Hu et al., 2015).

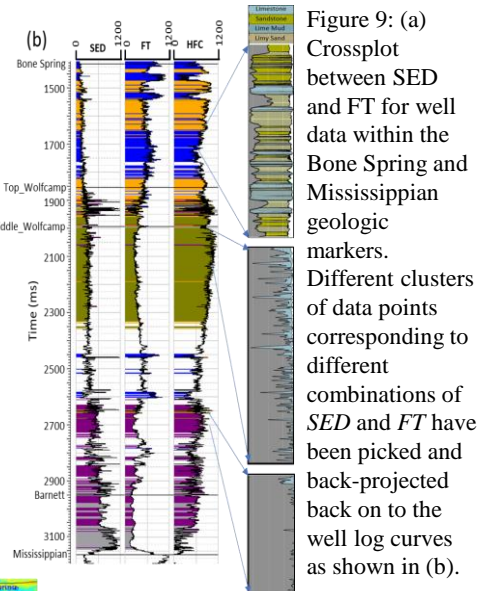


Figure 9: (a) Crossplot between SED and FT for well data within the Bone Spring and Mississippian geologic markers. Different clusters of data points corresponding to different combinations of SED and FT have been picked and back-projected back on to the well log curves as shown in (b).

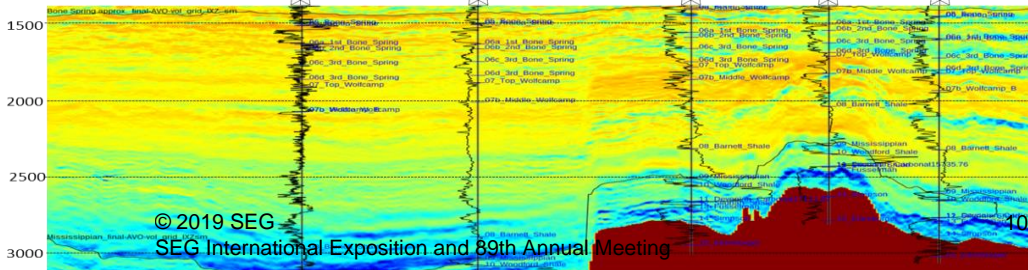


Figure 10: An arbitrary line passing through different wells extracted from the HFC volume. GR curves have been overlaid on the section. Within the Bone Spring, as we glance from left to right, we see the lowering of fracture toughness, which is possible due to the higher presence of carbonate content there.

REFERENCES

- Bai, M., 2016, Why are brittleness and fracability not equivalent in designing hydraulic fracturing in tight shale gas reservoirs: *Petroleum*, **2**, 1–19, doi: <https://doi.org/10.1016/j.petlm.2016.01.001>.
- Chopra, S., and R. K., Sharma, 2017, Misconceptions about brittleness and the talk about fracture toughness: *AAPG Explorer*, 20–21, August issue.
- Griffith, A. A., 1920, The phenomena of rupture and flow in solids: *Philosophical Transactions of the Royal Society B*, **221**, 163–198, doi: <https://doi.org/10.1098/rsta.1921.0006>.
- Griffith, A. A., 1924, The theory of rupture, in C. G. Biezeno, and J. M. Burgers, eds, *Proceedings of the 1st International Congress on Applied Mechanics*: Delft, Tech. Boekhandel en Drukkerij J. Waltman Jr., 54–63.
- Holt, R. M., E., Fjaer, O. M., Nes, and H. T., Alassi, 2011, A shaly look at brittleness: 45th US Rock Mechanics/Geomechanics Symposium, ARMA 11-366.
- Hu, Y., M. E. G., Perdomo, K., Wu, Z., Chen, K., Zhang, D., Ji, and H., Zhong, 2015, A novel model of brittleness index for shale gas reservoirs: confining pressure effect: SPE-176886, Society of Petroleum Engineers.
- Jarvie, D. M., R. J., Hill, T. E., Ruble, and R. M., Pollastro, 2007, Unconventional shale-gas systems: the Mississippian Barnett shale of north-central Texas as one model for thermogenic shale-gas assessment: *AAPG Bulletin*, **91**, 475–499, doi: <https://doi.org/10.1306/12190606068>.
- Jin, X., S. N., Shah, and J. C., Roegiers, 2015, An integrated petrophysics and geomechanics approach for fracability evaluation in shale reservoirs: *SPE Journal*, **20**, 518–526, doi: <https://doi.org/10.2118/168589-PA>.
- Lutz, S. J., S., Hickman, N., Davatzes, E., Zemach, P., Drakos, and A. R., Tait, 2010, Rock mechanical testing and petrologic analysis in support of well stimulation activities at the desert peak geothermal field, Nevada: *Proceedings of the 35th Workshop on Geothermal Reservoir Engineering*.
- Mathia, E., K., Ratcliffe, and M., Wright, 2016, Brittleness index– a parameter to embrace or avoid?: URTeC: 2448745.
- Miskimins, J. L., 2012, The impact of mechanical stratigraphy on hydraulic fracture growth and design consideration for horizontal wells: Search and Discovery Article #41102, available at http://www.searchanddiscovery.com/documents/2012/41102miskimins/ndx_miskimins.pdf, accessed on 11th March 2019.
- Rickman, R., M. J., Mullen, J. E., Petre, W. V., Grieser, and D., Kundert, 2008, A practical use of shale petrophysics for stimulation design optimization: All shale plays are not clones of the Barnett Shale: SPE 115258, Society of Petroleum Engineers.
- Sack, R. A., 1946, Extension of Griffith's theory of rupture to three dimensions: *Proceedings of the Physical Society of London*, **58**, 729–736, doi: <https://doi.org/10.1088/0959-5309/58/6/312>.
- Sharma, R. K., and S., Chopra, 2015, Determination of lithology and brittleness of rocks with a new attribute: *The Leading Edge*, **34**, 554–564, doi: <https://doi.org/10.1190/tle34050554.1>.
- Sneddon, I. N., 1946, The distribution of stress in the neighbourhood of a crack in an elastic solid: *Proceedings of the Royal Society, A*, **187**, 229–260, doi: <https://doi.org/10.1098/rspa.1946.0077>.
- Wang, F. P., and J. F., Gale, 2009, Screening criteria for shale-gas system: *Gulf Coast Association of Geological Societies (Trans Gulf Coast Assoc Geol Soc)*, **59**, 779–793.
- Yagiz, S., 2009, Assessment of brittleness using rock strength and density with punch penetration test: *Tunnelling and Underground Space Technology*, **24**, 16–74.
- Zhang, J. J., and L. R., Bentley, 2005, Factors determining Poisson's ratio: *CREWES Research Report*, **17**, 1–15.